High-accuracy high-mass-ratio simulations for binary neutron stars and their comparison to existing waveform models

Maximiliano Ujevic[,1] Alireza Rashti[,2] Henrique Gieg[,1] Wolfgang Tichy[,2] and Tim Dietrich[3,4]

[1]*Centro de Ciências Naturais e Humanas, Universidade Federal do ABC,*
09210-170, Santo André, São Paulo, Brazil
[2]*Department of Physics, Florida Atlantic University, Boca Raton, Florida 33431, USA*
[3]*Institut für Physik und Astronomie, Universität Potsdam, Haus 28,*
Karl-Liebknecht-Straße 24/25, D-14476, Potsdam, Germany
[4]*Max Planck Institute for Gravitational Physics (Albert Einstein Institute),*
Am Mühlenberg 1, Potsdam 14476, Germany

The subsequent observing runs of the advanced gravitational-wave detector network will likely provide us with various gravitational-wave observations of binary neutron star systems. For an accurate interpretation of these detections, we need reliable gravitational-wave models. To test and to point out how existing models could be improved, we perform a set of high-resolution numerical relativity simulations for four different physical setups with mass ratios $q = 1.25$, 1.50, 1.75, 2.00, and total gravitational mass $M = 2.7 \ M_\odot$. Each configuration is simulated with five different resolutions to allow a proper error assessment. Overall, we find approximately second-order converging results for the dominant (2,2) mode, but also the subdominant (2,1), (3,3), and (4,4) modes, while generally, the convergence order reduces slightly for an increasing mass ratio. Our simulations allow us to validate waveform models, where we find generally good agreement between state-of-the-art models and our data, and to prove that scaling relations for higher modes currently employed for binary black hole waveform modeling also apply for the tidal contribution. Finally, we also test if the current NRTidal model used to describe tidal effects is a valid description for high-mass-ratio systems. We hope that our simulation results can be used to further improve and test waveform models in preparation for the next observing runs.

I. INTRODUCTION

The detection of GW170817 [1–3] and the connected electromagnetic counterparts revolutionized astronomy. This observation of a binary neutron star (BNS) merger led to a variety of important scientific results—e.g., new constraints on the nature of matter at supranuclear densities [4–18], an independent measurement of the Hubble constant [17,19–21], the confirmation that BNSs are a possible central engine for short gamma-ray bursts (GRBs) [22], and the proof that BNSs are a production fabric for heavy elements [23–29]. In contrast to GW170817, the second BNS detection, GW190425 [30], was not accompanied by any electromagnetic signature. Likely, this was caused by the large total mass of GW190425, which was larger than the masses of BNS systems previously observed in our Galaxy [31]. Given the unexpected large total mass of GW190425, it might also seem plausible that upcoming gravitational-wave (GW) detections will originate from BNS systems with mass ratios that differ noticeably from the more common equal mass case.

Theoretically, the expected NS mass ranges within $(1.0 - 2.3) \ M_\odot$. Bounds on the minimum mass of NSs

come from the NS formation scenario (gravitational collapse) and from observations of low-mass NSs [32,33], despite the fact that such measurements typically have large uncertainties. A lower bound on the maximum NS mass arises from Shapiro-time-delay measurements of massive pulsars such as PSR $J0348 + 0432$ [34], PSR $J1614 - 2230$ [35], and PSR $J0740 + 6620$ [36,37]. Contrarily, the interpretation that the BNS merger GW170817 formed a black hole (BH) [7,38–40] provides an upper bound on the maximum NS mass; cf. Ref. [17] for a more complete assessment of the NS maximum-mass posterior distribution. Based on these considerations, the theoretical upper bound on the mass ratio of a BNS system is about $q = M_1/M_2 \lesssim 2.3$.

Comparing this theoretical limit to the observed population of BNSs in our galaxy, one finds that none of the observed systems has such a large mass ratio. In fact, most BNS clusters are around the equal mass case [41], but there are discoveries about compact binary systems with mass ratios of $q \approx 1.3$ (e.g., Refs. [42,43]). Hence, BNSs with larger mass ratios might exist, and our current sample of observed BNS systems is simply too limited. Similarly,

population synthesis studies predict a wider range of masses and mass ratios up to $q \approx 1.9$ (e.g., Ref. [44]). Given the rising field of GW astronomy and the uncertainty in the mass ratio of upcoming BNS detections, a careful investigation of GW signals from high-mass-ratio systems seems necessary.

Overall, the analysis of GW signals requires accurate theoretical models that can be cross-correlated with the observational data. Such models have to be sufficiently fast to ensure that several million templates for various binary parameters can be compared to the observational data. For BNS systems, the existing GW models can be classified into three categories: analytical post-Newtonian (PN) models (cf. Ref. [45] and references therein), semianalytical waveforms based on the effective one-body (EOB) approach [46–53], and phenomenological approximants [54–57]; cf. Ref. [58] for a recent review on how to model GWs from BNS systems. All of these models (PN, EOB, and phenomenological) have benefits and drawbacks. While PN models are fast to compute, given that only an algebraic expression has to be evaluated to obtain the full waveforms, they become increasingly inaccurate when the distance between the two compact objects reduces (e.g., Refs. [56,59,60], but see also Ref. [61] for recent analysis of GW170817 and GW190425 with PN models). Contrarily, the EOB approach [62,63] allows us to overcome this accuracy issue by remapping the relativistic two-body system into an effective one-body problem. However, due to this approach, the pure time-domain EOB models are typically too slow to be directly used for parameter estimation, such that one has to either construct reduced-order models (e.g., Refs. [64,65]), use the adiabatic approximation (e.g., Refs. [53,66,67]), or employ alternative parameter estimation methods (e.g., Ref. [68]). Finally, phenomenological models focus on providing algebraic expressions—i.e., they are quick to evaluate, and they combine PN, EOB, and also NR information in ways such that unknown higher-order PN parameters are fitted to EOB and NR data. Numerous studies have investigated the effect of using different waveform models on GW parameter estimation (e.g., Refs. [69–75]).

To develop and validate these models, one requires numerical relativity (NR) simulations for an accurate description of the merger process based on first principles. While there have been several studies addressing the effect of high mass ratios on the dynamics and merger process (e.g., Refs. [76–80]), there exists only a limited set of simulations usable for GW model development—i.e., simulations using eccentricity-reduced initial data and with an accurate error estimate for the GW phase based on a clear convergence. In this article, we will overcome these limitations and produce a small set of highly accurate simulations. We have simulated a total of four physical systems with mass ratios $q = 1.25, 1.50, 1.75,$ and 2.00 and a fixed total mass of $M = 2.7\ M_\odot$. We will use this new set

of simulations to study the performance of existing GW models for such large mass ratios and will further investigate if techniques employed for modeling the higher-order modes in binary black hole models could also be used for the tidal contributions of the GW phase.

Throughout this work, we use geometric units, setting $c = G = M_\odot = 1$, though we will sometimes include $M_\odot$ explicitly or quote values in CGS units for better understanding.

II. METHODS

A. Numerical setups

Our numerical simulations are based on SGRID initial data [81–84]. SGRID is a pseudospectral code that employs surface fitting coordinates to solve the Einstein constraint equations using the extended conformal thin sandwich formulation [85], and it employs the constant rotational velocity approach to describe the NSs with arbitrary rotational profiles [82,86].

The dynamical evolutions are performed with the BAM code [87–91]. BAM uses the Z4c formulation [92,93] of the Einstein equations along with $1 + \log$ and gamma-driver shift conditions [94–96] for the gauge evolution. Matter variables are evolved using the $3 + 1$-conservative Eulerian formulation of general relativistic hydrodynamics (GRHD). The system of equations is closed by an equation of state (EOS) that is a piecewise polytropic fit for the SLy [97] EOS, which is in broad agreement with recent multimessenger constraints, with an additional thermal contribution to the pressure given by $p_{\rm th} = (\Gamma_{\rm th} - 1)\rho$, where we set $\Gamma_{\rm th} = 1.75$ [98].

BAM's numerical domain is divided into a hierarchy of cell-centered nested Cartesian grids consisting of L levels labeled by $l = 0, \ldots, L - 1$. Each level l contains one or more Cartesian boxes with constant grid spacing h_l and n (or $n^{\rm mv}$) number of points per direction. The resolution in each level is given as $h_l = h_0/2^l$. Higher levels $l \geq l_{\rm mv}$ move dynamically according to the technique of "moving boxes" and follow the motion of the neutron stars. An overview about the grid configuration for different resolutions is given in Table I, where the outer boundary of the computational domain is set at the radius $R_0 \approx 1020\ M_\odot$.

B. Configurations

For this work, we prepare a set of four different physical BNS systems. Each setup has the same total gravitational mass in isolation but different mass ratios (see Table II). In order to eliminate eccentric contributions of the orbit to the gravitational wave during the inspiral, we perform between three and four steps of the eccentricity reduction procedure [83,99], obtaining values lower than 3.5×10^{-4}. All configurations start at the same initial frequency, and the number of orbits before merger is approximately 16. See Table III for important parameters characterizing the initial properties of the binaries.

TABLE I. Grid configurations. The columns refer to the resolution name, the number of levels L, the number of moving box levels L_{mv}, the number of points in the nonmoving boxes n, the number of points in the moving boxes n_{mv}, the grid spacing in the finest level h_6 covering the neutron star, and the grid spacing in the coarsest level h_0. The grid spacing is given in units of $M_\odot$.

Name	L	L_{mv}	n	n_{mv}	h_6	h_0
R1	7	4	128	64	0.249	15.936
R2	7	4	192	96	0.166	10.624
R3	7	4	256	128	0.1245	7.968
R4	7	4	384	192	0.083	5.312
R5	7	4	512	256	0.06225	3.984

TABLE II. Properties of the individual stars used for our BNS simulations. The first column gives the configuration name, and the second column gives the employed mass ratio $q = M^A/M^B \geq 1$, while the next four columns give the gravitational masses of the individual stars $M^{A,B}$ and the baryonic masses of the individual stars $M_b^{A,B}$.

Name	q	M^A	M^B	M_b^A	M_b^B
$S_{1.25}$	1.25	1.5001	1.2001	1.6834	1.3117
$S_{1.50}$	1.50	1.6201	1.0801	1.8388	1.1688
$S_{1.75}$	1.75	1.7183	0.9819	1.9695	1.0542
$S_{2.00}$	2.00	1.8002	0.9001	2.0813	0.9601

TABLE III. Properties of our BNS simulations. The columns give the configuration name, the residual eccentricity e, the initial GW frequency $M\omega_{2,2}^0$ of the (2,2) mode, the Arnowitt-Deser-Misner (ADM) mass M_{ADM}, and the angular momentum J_{ADM}. All configurations were evolved with the resolutions of Table I.

Name	e [10^{-4}]	$M\omega_{2,2}^0$ [10^{-2}]	M_{ADM}	J_{ADM}
$S_{1.25}$	1.6413	3.2241	2.6804	7.9252
$S_{1.50}$	3.0940	3.2231	2.6809	7.7035
$S_{1.75}$	3.1148	3.2220	2.6816	7.4280
$S_{2.00}$	3.4273	3.2213	2.6824	7.1353

III. RESULTS

A. Gravitational waves

We extract GWs from our simulations using the Newman-Penrose formalism [100] based on the curvature scalar Ψ_4. The GW strain is then computed from $\Psi_4 = \ddot{h}$, where we use the frequency domain integration outlined in Ref. [101]. For our purpose, it is convenient to decompose Ψ_4 as well as h into individual modes by employing spherical harmonics with spin weight -2—i.e.,

$$h = \sum_{l=2}^{l_{max}} \sum_{m=-l}^{m \leq l} {}^{-2}Y_{l,m} h_{l,m}. \tag{1}$$
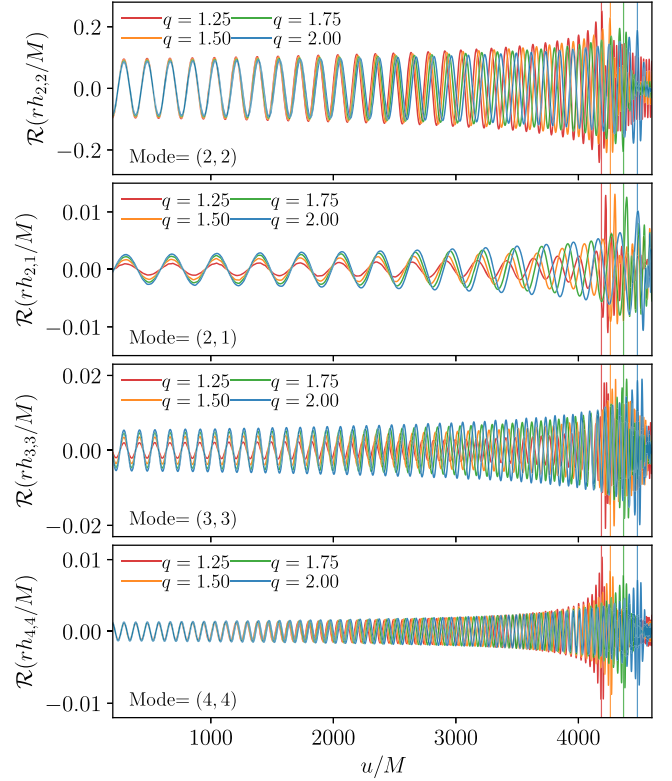

FIG. 1. Real part for different modes of the GW rh as a function of the retarded time u/M, where r is the coordinate radius. As expected, the (2,2) mode is the dominant mode, and the amplitudes of the (2,1) mode and (3,3) mode increase with increasing mass ratio. The vertical lines in the plot indicate the merger time for resolution R5, from which we note that systems with higher mass ratios starting at the same frequency merge later.

In Fig. 1, we show the dominant (2,2) mode of the GW signal in the top panel and the subdominant (2,1), (3,3), and (4,4) modes in the following rows. For completeness, we want to summarize some of the main findings that, however, have already been found by previous studies and also analytical computations (e.g., Ref. [45]).

(i) The (2,2) mode is dominant and has the largest amplitude.

(ii) The amplitudes of all the (l, m) modes with odd m values increase with increasing mass ratio. In the equal-mass case, due to the symmetry of the system, these modes are zero (during the inspiral).

(iii) The frequencies of the individual modes depend on the value of $|m|$ and scale roughly according to $\omega_{2,2} \cdot |m/2|$.

(iv) For nonprecessing systems, the m and $-m$ modes are identical (not shown in Fig. 1).

B. Convergence properties

To investigate the convergence properties of our simulations, we write the GWs as

$$h_{l,m} = A_{l,m} e^{-i\phi_{l,m}}, \qquad (2)$$

with the amplitude $A_{l,m}$ and the phase $\phi_{l,m}$. Given that GW astronomy relies mainly on a proper estimate of the GW phase, we will focus our discussion on the convergence properties for the GW phase. For this purpose, we show the convergence of all modes (for all setups and resolutions) in Fig. 2. Based on our previous studies [90,102], we expect to obtain second-order convergence for our numerical simulations with respect to the (2,2) mode.

In this work, we tested that this convergence order is also present in the higher-order modes. For this purpose, we scale the phase difference between two different resolutions under the assumption of second-order convergence and find good agreement for the high-resolution simulations. Let us outline key features of the plot:

(i) Phase differences with respect to the lowest resolution R1 indicate that for such a resolution, the simulations do not reach the convergent regime. Hence, a smaller grid spacing—i.e., a higher resolution—is required.

(ii) Independent of the mode that we consider, an increasing mass ratio leads to a slight reduction of the convergence order.

(iii) Due to the very small amplitude, the assessment of the convergence properties for the (2,1) mode is problematic for mass ratios below $q = 1.75$ (cf. Fig. 1).

In addition to the phase difference between individual resolutions, we also show the difference between the GW phase for the highest resolution and Richardson-extrapolated waveforms for which we assumed second-order convergence during the extrapolation; see Refs. [90,102] for more details about this procedure.

C. Tidal contribution in higher modes

Several GW models that model higher-order modes start from a description of the dominant (2,2) mode and then rescale this mode to obtain subdominant mode predictions (e.g., Refs. [103–105]). The scaling relations are

$$\phi_{l,m} = m\phi_{\text{orbital}} + \Delta\phi_{l,m} \qquad (3)$$
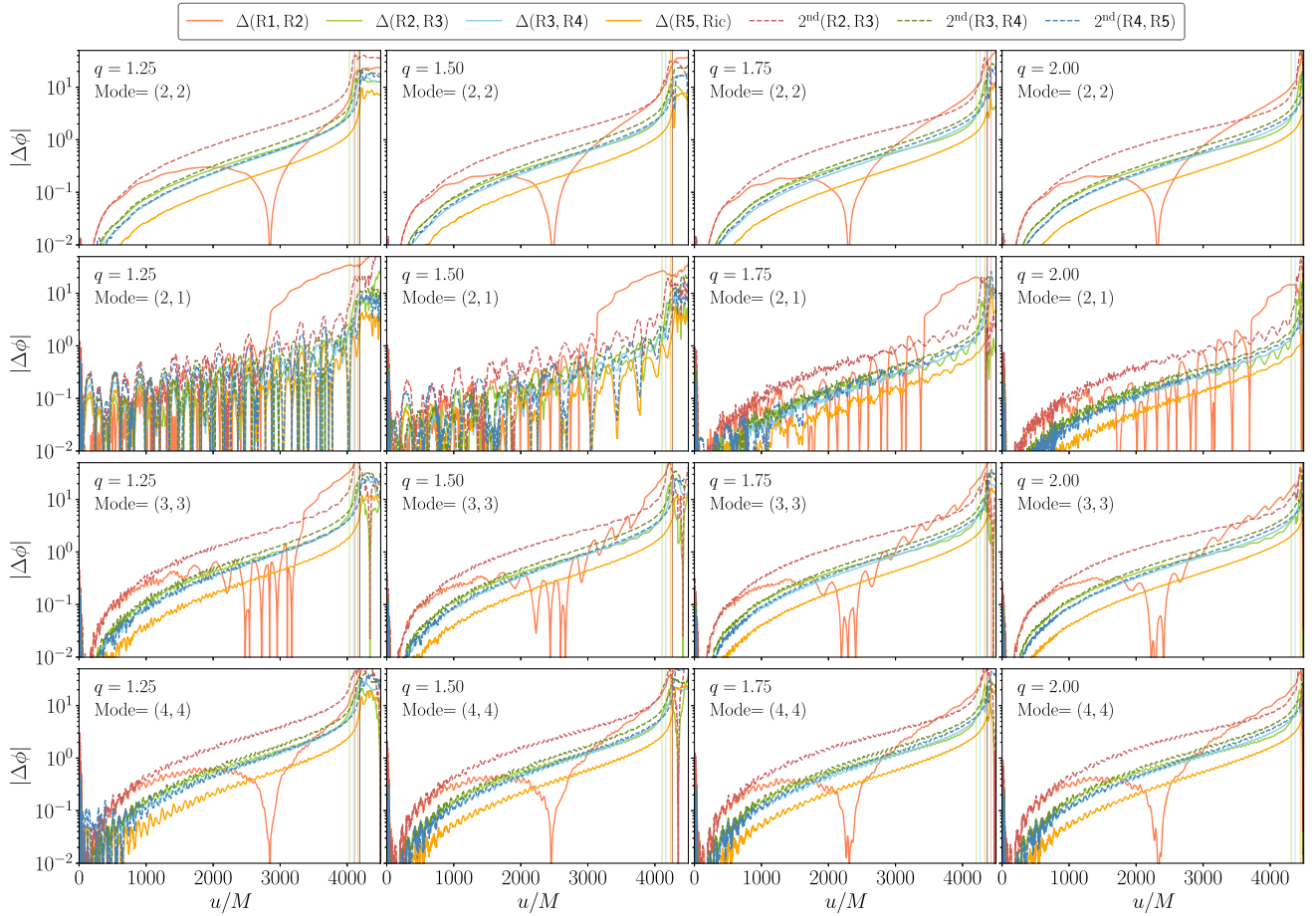

FIG. 2.   Convergence for all important modes. We show the phase differences between different resolutions (solid lines) and the rescaled phase differences assuming second-order convergence (dashed lines). Individual rows refer to the (2,2), (2,1), (3,3), and (4,4) modes (from top to bottom), and the individual columns refer to the setups with increasing mass ratio. The vertical lines in the plot indicate the merger time.

with the orbital phase ϕ_{orbital} and

$$\Delta\phi_{2,2} \rightarrow 0, \quad \Delta\phi_{2,1} \rightarrow \pi/2, \quad \Delta\phi_{3,3} \rightarrow -\pi/2, \quad \Delta\phi_{4,4} \rightarrow \pi.$$
(4)

Under the assumption of $2\phi_{\mathrm{orbital}} \approx \phi_{2,2}$, this allows us to use information from the dominant (2,2) mode to predict the evolution of the subdominant modes. As expected, this scaling relation also clearly applies for our NR simulations using the highest-resolution data. This becomes visible in Fig. 3, where we rescale the (2,2)-mode contribution according to Eqs. (3) and (4) and find overall perfect agreement between our data and the analytical predictions.

In addition to the investigation of the entire mode content, we also want to investigate if the rescaling can be applied to the individual contributions—see Eq. (5). Overall, also for the individual contributions, our NR simulations can serve as a validation set, and they prove that BNS simulations can reach an accuracy level where the reliable modeling of subdominant modes becomes possible.

An approach that is intensively used during the modeling of BNS and BHNS systems is the assumption that the GW phase can be decomposed into different components. Keeping for simplicity the (2,2) mode, we get

$$\phi_{2,2} = \phi_{2,2}^{\mathrm{BBH}} + \phi_{2,2}^{\mathrm{SO}} + \phi_{2,2}^{\mathrm{SS}} + \phi_{2,2}^{\mathrm{Tidal}} + \cdots,$$
(5)

with the nonspinning BBH contribution $\phi_{2,2}^{\mathrm{BBH}}$, the spin-orbit contributions $\phi_{2,2}^{\mathrm{SO}}$, the spin-spin contribution $\phi_{2,2}^{\mathrm{SS}}$, and the tidal contributions $\phi_{2,2}^{\mathrm{Tidal}}$. In this article, we will particularly focus on $\phi_{2,2}^{\mathrm{Tidal}}$, as well as higher-order

contributions $\phi_{2,1}^{\mathrm{Tidal}}$, $\phi_{3,3}^{\mathrm{Tidal}}$, and $\phi_{4,4}^{\mathrm{Tidal}}$; the spin contributions are zero in our spinless configurations. For this purpose, we subtract from our BNS NR waveforms the BBH contributions computed with the SEOBNRv4T [47] model (in its form currently implemented in LALSuite [106]).

Figure 4 summarizes our findings: The scaling relations of Eq. (3) also apply for the tidal contribution. This is of special importance for the possibility to extend existing BNS or BHNS models that currently purely model the dominant (2,2) mode (e.g., Refs. [56,57,107,108]), to model the tidal contributions present in higher modes.

IV. COMPARISON WITH EXISTING GW MODELS

A. Model validation

An important application for our new NR simulations is the possibility to quantify the performance of GW models currently employed in GW analysis. For this purpose, we compare our simulation results with five different state-of-the-art GW models—namely, SEOBNRv4T [47], TEOBResumS [49,50], SEOBNRv4_ROM_NRTidalv2 [57], IMRPhenomPv2_NRTidal [56], and IMRPhenomPv2_NRTidalv2 [57]. For completeness, we summarize key features of each model in the Appendix.

In Fig. 5, we show the phase difference between the GWs obtained from different GW models and the Richardson-extrapolated signal. Before subtracting, we first align the model waveform with respect to the Richardson-extrapolated data by minimizing their phase difference on an early stage of the inspiral, where $M\omega_{2,2} \in [0.035, 0.040]$. For comparison, we also show in the figure two different error bands. The conservative light gray error band ($\pm\epsilon$) is estimated using two terms—i.e., $\epsilon^2 = \epsilon_{\mathrm{Ric}}^2 + \epsilon_{\mathrm{Ext}}^2$. The first term is obtained through the difference between the Richardson-extrapolated value and the NR simulation with the highest resolution—i.e.,
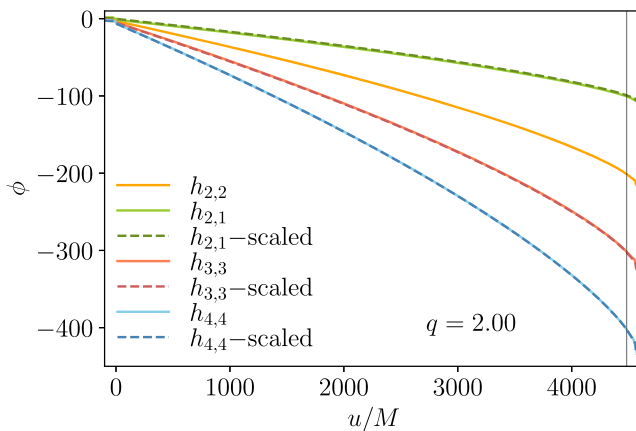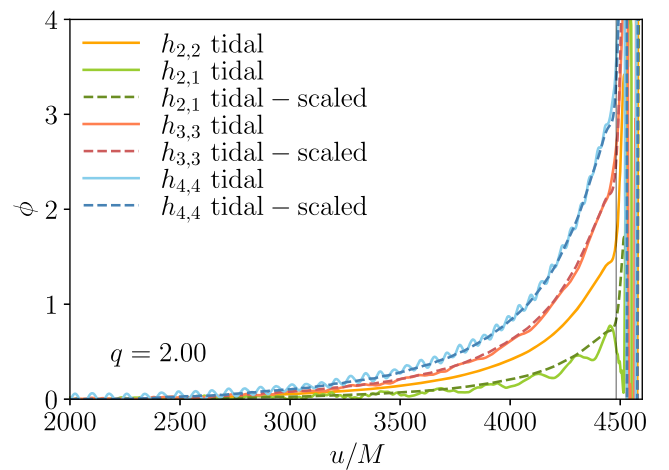

FIG. 3. Accumulated phase of our simulations for the $q = 2.00$ setup, where we show the individual modes with different colors and rescale the dominant (2,2) mode according to the description given in the text to mirror the evolution of the subdominant modes. The scaling of the accumulated phase is verified for all mass ratios.

FIG. 4. Rescaling of the tidal contribution $\phi_{l,m}^{\mathrm{Tidal}}$ for different modes similar to Fig. 3 for the entire phase contribution of each mode. We verify that the scaling of the tidal contribution is valid for all mass ratios.
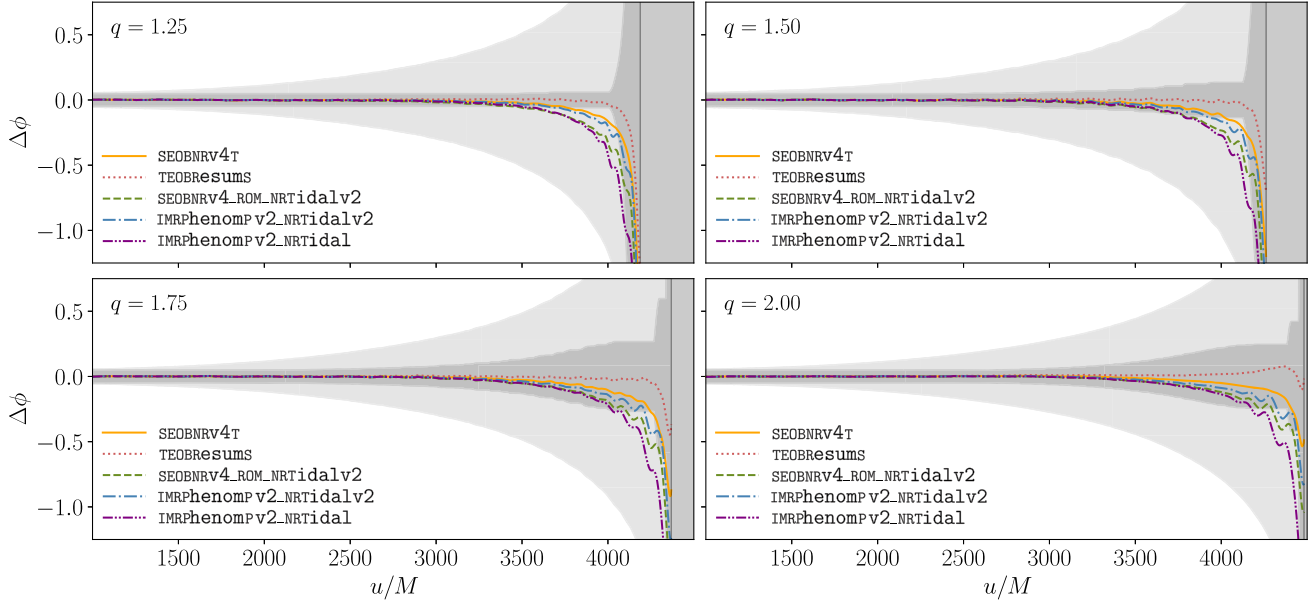
FIG. 5. Phase difference of the (2,2) mode between the Richardson-extrapolated data and the different GW models for all values of q. The alignments of their phases have been performed on an early stage in the inspiral before subtracting. All GW models fall within our more conservative light gray error band.

$\epsilon_{\mathrm{Ric}} = \Delta(\mathrm{Ric} - \mathrm{R5})$. The second term, ϵ_{Ext}, is obtained by calculating the phase difference between two different extraction radii. In our case, we consider the radii $700\,M_{\odot}$ and $900\,M_{\odot}$ in the highest resolution available. This last term is almost constant and is the dominant error in ϵ until approximately $2000\,M_{\odot}$. The dark gray error band ($\pm\epsilon_{\Delta}$) is an error for the third-order Richardson extrapolation itself, and it is given by $\epsilon_{\Delta}^2 = \max[\epsilon_{\Delta\mathrm{Ric}}^2 + \epsilon_{\mathrm{Ext}}^2]$, where "max" indicates that we are keeping the highest value as time passes by, to ensure a monotonically increasing uncertainty. The first term, $\epsilon_{\Delta\mathrm{Ric}}$, is the difference between two different Richardson extrapolations. One extrapolation is done with resolutions R3 and R4, Ric_{34}, and the other one with resolutions R4 and R5, Ric_{45}. Thus, this term can be written as $\epsilon_{\Delta\mathrm{Ric}} = \Delta(\mathrm{Ric}_{45} - \mathrm{Ric}_{34})$. The second term is the same present in ϵ. In this case, $\epsilon_{\Delta\mathrm{Ric}}$ becomes larger than ϵ_{Ext} only in the final stage of the inspiral.

Independent of the mass ratio, we find that the phase differences between our Richardson-extrapolated waveforms and the waveform approximants are in good agreement. All models fall within our more conservative error measure ϵ and therefore can not be clearly discarded/disfavored in any way. Nevertheless, we do find interesting patterns in our analysis. Noticeably, the IMRPhenomPv2_NRTidal model shows the largest difference from our NR-based data. The two NRTidalv2 models IMRPhenomPv2_NRTidalv2 and SEOBNRv4_ROM_NRTidalv2 perform slightly better. However, all models fall shortly before merger out of our tighter error band ϵ_{Δ} (cf. the dark gray region). The two time-domain EOB models SEOBNRv4T and TEOBResumS perform best with, in particular, TEOBResumS always staying within our tight

error band. Interestingly, in general, we find that the phase difference between our prediction and the GW model predictions is negative—i.e., Richardson-extrapolated values (third order) minus Model. The only exception to this "rule" is the simulation for the highest mass ratio, where TEOBResumS shows a positive phase difference with respect to our NR data close to merger. While one could speculate that this is caused by an overestimation of tidal effects for TEOBResumS for large mass ratios, it is more likely that this is caused by the fact that the Richardson-extrapolated result is
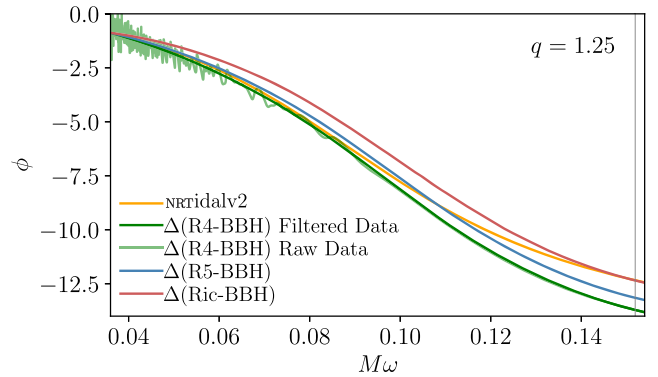

FIG. 6. Tidal contributions of the (2,2) mode of our NR simulations and the Richardson-extrapolated data for the case $q = 1.25$. For comparison, we align them with the NRTidalv2 tidal model. To show the effect of the filtering procedure on the results, we present the R4 configuration with (dark green) and without (light green) the Savitzky-Golay filtering.
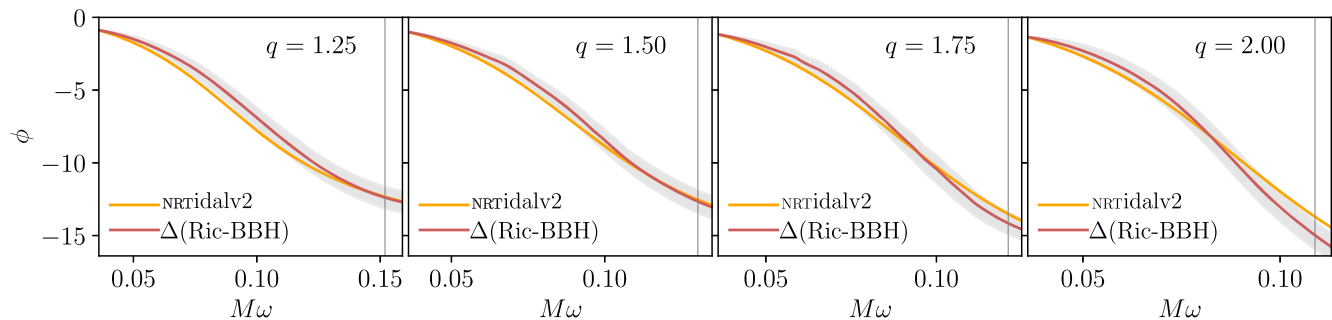
FIG. 7. Comparison of the NRTidalv2 model (orange) with the tidal contribution of the (2,2) mode of the Richardson-extrapolated data (brown) for all values of q. In general, the model has some deviations but behaves correctly for all mass ratios and falls within our error band during most of the frequency interval.

less accurate, since the convergence order reduces slightly before the merger, as seen in Fig. 2.

B. Outlooks to improve the NRTidal model

In addition to the general model comparison presented in the previous subsection, we want to focus on the potential to further improve (and test) the NRTidal description [54]. In general, the NRTidal phase contribution, used to augment existing BBH models, is based on the possibility to extract $\phi(\omega)$. So far, only the (2,2) mode has been used for any NRTidal-based model, but based on Fig. 4, higher modes could also be modeled. Hereafter for simplicity, we use ω to refer to $\omega_{2,2}$.

Another important point is that, while the NRTidalv2 model incorporated next-to-leading-order mass-ratio effects, the model has been calibrated purely to equal-mass simulations; see Ref. [57]. To check the robustness of this approach, we first extract the tidal contribution to $\phi_{2,2}(\omega)$ from our simulations.

To obtain the tidal contribution $\phi_{2,2}^{\text{Tidal}}(\omega)$ from the NR simulation, we need to subtract the BBH contribution $\phi_{2,2}^{\text{BBH}}(\omega)$ from $\phi_{2,2}(\omega)$. As a first step, we again use SEOBNRv4T to model $\phi(t)$ for a BBH system with the same component masses. Then, we can calculate $\omega = \partial_t \phi$ and obtain $\phi(\omega)$. Afterwards, we align the BBH phase and the BNS phase at a given frequency, where we use here $M\omega = 0.036$ as the reference frequency for alignment. Finally, after obtaining the tidal contribution, we perform a further alignment with the NRTidalv2 model using the same reference frequency. The tidal contributions $\phi_{2,2}^{\text{Tidal}}(\omega)$ found in this way have an oscillatory behavior for low frequencies. To reduce these oscillations, we employ the Savitzky-Golay filtering. In Fig. 6, we present, for the $q = 1.25$ case, the tidal contributions $\phi_{2,2}^{\text{Tidal}}(\omega)$ for different NR resolutions and for the Richardson-extrapolated waveform. In dark and light green we show an example of the use of the Savitzky-Golay filtering—the original tidal contribution for resolution R4 (light green) has an oscillatory behavior near $M\omega = 0.04$, which is

corrected after using the filtering (dark green). For resolutions R5 and Ric, we plot only the filtered version.

In Fig. 7, we compare the tidal contribution of the Richardson-extrapolated waveform, $\phi_{2,2\,\text{Ric}}^{\text{Tidal}}(\omega)$, with the NRTidalv2 model for different mass ratios. Each tidal contribution is obtained following the procedure described in the above paragraph. The error band in these plots is calculated using the difference between the Richardson-extrapolated value and the highest NR resolution—i.e., $\epsilon^{\text{Tidal}} = \pm\Delta[\phi_{2,2\,\text{Ric}}^{\text{Tidal}}(\omega) - \phi_{2,2\,\text{R5}}^{\text{Tidal}}(\omega)]$. Taking into account this conservative error, we see that in general, the NRTidalv2 model behaves correctly for all mass ratios and falls within our error band during most of the frequency interval. However, there are deviations. These are most noticeable for $q = 1.25$ (at the frequency $M\omega \approx 0.08$) and for $q = 2.00$ (at frequencies $M\omega > 0.08$). Because of this, we still see room for improvement of the NRTidal phase description, and we hope that our new set of NR data will be helpful towards future development.

V. CONCLUSION AND OUTLOOK

In this article, we have performed simulations of four different BNS systems for mass ratios $q = 1.25, 1.50, 1.75$, and 2.00. All physical configurations have been simulated with five different resolutions to allow for a proper error assessment. We find that the (2,2), (2,1), (3,3), and (4,4) modes show second-order convergence, where for larger mass ratios the convergence order drops slightly around the moment of merger. We use our simulations to compute Richardson-extrapolated GW data that we compare against existing, state-of-the-art GW models. We find overall good agreement (within our estimated error bands), but a preference for the models TEOBResumS and SEOBNRv4T.

Our simulations allow us also to verify that the estimated tidal contribution to the dominant (2,2) mode can be rescaled to mimic tidal contributions for the subdominant modes. This is of special interest for the development of future BNS and BHNS models that will be required for the upcoming observing runs of the advanced GW detector networks.

Finally, we verify that despite the calibration to equal-mass systems, the existing NRTidalv2 model is able to describe also high-mass-ratio systems as presented here. Nevertheless, we expect that based on this set of simulations and upcoming simulations that are ongoing, there will be the possibility to further improve the NRTidal model to ensure a more reliable interpretation of future GW signals.

APPENDIX: SUMMARY OF EMPLOYED GW MODELS

IMRPhenomPv2_NRTidal is based on the precessing BBH model IMRPhenomPv2 [109,110] and uses the original NRTidal correction [54,56] to account for tidal contributions. In addition, 2PN and 3PN EOS-dependent spin-spin effects are employed to augment the existing BBH baseline model. No further tidal amplitude corrections are employed.

IMRPhenomPv2_NRTidalv2 is an update of IMRPhenomPv2_NRTidal. In addition to IMRPhenomPv2_NRTidal, this model uses the updated NRTidalv2 [56] description for the tidal contribution. It also employs a tidal amplitude correction, and it includes up to 3.5 PN EOS-dependent effects in the spin-spin and cubic-in-spin contributions (including octupole-dependent terms).

SEOBNR_ROM_NRTidalv2 is a frequency domain model based on the surrogate SEOBNRv4_ROM [65,111]. The BBH model is augmented with the NRTidalv2 phase corrections [56], uses tidal amplitude corrections, and includes EOS-dependent spin-spin and cubic-in-spin corrections up to 3.5 PN.

SEOBNRv4T is a time domain EOB model [47,48] based on the time domain BBH model [111]. The model includes quadrupolar and octupolar dynamical tides, as well as EOS-dependent spin-induced quadrupole moment effects. In our work, we rely on the publicly available version of LALSuite [47] that does not include the spin dependence of the dynamical tidal effects as presented in Ref. [112].

TEOBResumS is a time domain EOB model. In contrast to SEOBNRv4T, TEOBResumS uses gravitational self-force-inspired expressions for the attractive tidal potential [51] but is restricted to adiabatic tidal effects. As for the other models, we rely on the publicly available TEOBResumS model that is part of LALSuite [49,50].

[1] B. P. Abbott *et al.* (Virgo and LIGO Scientific Collaborations), Phys. Rev. Lett. **119,** 161101 (2017).

[2] B. P. Abbott *et al.* (LIGO Scientific, Virgo, Fermi GBM, INTEGRAL, IceCube, AstroSat Cadmium Zinc Telluride Imager Team, IPN, Insight-Hxmt, ANTARES, Swift, AGILE Team, 1M2H Team, Dark Energy Camera GW-EM, DES, DLT40, GRAWITA, Fermi-LAT, ATCA, AS-KAP, Las Cumbres Observatory Group, OzGrav, DWF (Deeper Wider Faster Program), AST3, CAASTRO, VINROUGE, MASTER, J-GEM, GROWTH, JAGWAR, CaltechNRAO, TTU-NRAO, NuSTAR, Pan-STARRS, MAXI Team, TZAC Consortium, KU, Nordic Optical Telescope, ePESSTO, GROND, Texas Tech University, SALT Group, TOROS, BOOTES, MWA, CALET, IKI-GW Follow-up, H.E.S.S., LOFAR, LWA, HAWC, Pierre Auger, ALMA, Euro VLBI Team, Pi of Sky, Chandra Team at McGill University, DFN, ATLAS Telescopes, High Time Resolution Universe Survey, RIMAS, RATIR, SKA South Africa/MeerKAT Collaborations), Astrophys. J. Lett. **848,** L12 (2017).

[3] B. P. Abbott *et al.* (Virgo, Fermi-GBM, INTEGRAL, LIGO Scientific Collaborations), Astrophys. J. **848,** L13 (2017).

[4] E. Annala, T. Gorda, A. Kurkela, and A. Vuorinen, Phys. Rev. Lett. **120,** 172703 (2018).

[5] A. Bauswein, O. Just, H.-T. Janka, and N. Stergioulas, Astrophys. J. **850,** L34 (2017).

[6] F. J. Fattoyev, J. Piekarewicz, and C. J. Horowitz, Phys. Rev. Lett. **120,** 172702 (2018).

[7] M. Ruiz, S. L. Shapiro, and A. Tsokaros, Phys. Rev. D **97,** 021501 (2018).

[8] M. Shibata, S. Fujibayashi, K. Hotokezaka, K. Kiuchi, K. Kyutoku, Y. Sekiguchi, and M. Tanaka, Phys. Rev. D **96,** 123012 (2017).

[9] D. Radice, A. Perego, F. Zappa, and S. Bernuzzi, Astrophys. J. **852,** L29 (2018).

[10] S. De, D. Finstad, J. M. Lattimer, D. A. Brown, E. Berger, and C. M. Biwer, Phys. Rev. Lett. **121,** 091102 (2018).

[11] E. R. Most, L. R. Weih, L. Rezzolla, and J. Schaffner-Bielich, Phys. Rev. Lett. **120,** 261103 (2018).

[12] C. D. Capano, I. Tews, S. M. Brown, B. Margalit, S. De, S. Kumar, D. A. Brown, B. Krishnan, and S. Reddy, Nat. Astron. **4,** 625 (2020).

[13] B. P. Abbott *et al.* (LIGO Scientific and Virgo Collaborations), Phys. Rev. X **9,** 011001 (2019).

[14] B. P. Abbott *et al.* (Virgo, LIGO Scientific Collaborations), Phys. Rev. Lett. **121,** 161101 (2018).

[15] M. W. Coughlin, T. Dietrich, Z. Doctor, D. Kasen, S. Coughlin, A. Jerkstrand, G. Leloudas, O. McBrien, B. D. Metzger, R. O'Shaughnessy, and S. J. Smartt, Mon. Not. R. Astron. Soc. **480,** 3871 (2018).

[16] M. W. Coughlin, T. Dietrich, B. Margalit, and B. D. Metzger, Mon. Not. R. Astron. Soc. **489,** L91 (2019).

[17] T. Dietrich, M. W. Coughlin, P. T. H. Pang, M. Bulla, J. Heinzel, L. Issa, I. Tews, and S. Antier, Science **370,** 1450 (2020).

[18] S. Huth *et al.*, Nature (London) **606,** 276 (2022).

[19] B. P. Abbott *et al.* (LIGO Scientific, VINROUGE, Las Cumbres Observatory, DLT40, Virgo, 1M2H, and MASTER Collaborations), Nature (London) **551,** 85 (2017).

[20] K. Hotokezaka, E. Nakar, O. Gottlieb, S. Nissanke, K. Masuda, G. Hallinan, K. P. Mooley, and A. Deller, Nat. Astron. **3,** 940 (2019).

[21] E. Nakar and T. Piran, Astrophys. J. **909,** 114 (2021).

[22] LIGO Scientific Collaboration *et al.*, Astrophys. J. **848,** L12 (2017).

[23] B. P. Abbott *et al.* (Virgo and LIGO Scientific Collaborations), Astrophys. J. **850,** L39 (2017).

[24] P. S. Cowperthwaite *et al.*, Astrophys. J. **848,** L17 (2017).

[25] S. J. Smartt *et al.*, Nature (London) **551,** 75 (2017).

[26] M. M. Kasliwal *et al.*, Science **358,** 1559 (2017).

[27] D. Kasen, B. Metzger, J. Barnes, E. Quataert, and E. Ramirez-Ruiz, Nature **551,** 80 (2017).

[28] D. Watson *et al.*, Nature (London) **574,** 497 (2019).

[29] S. Rosswog, J. Sollerman, U. Feindt, A. Goobar, O. Korobkin, R. Wollaeger, C. Fremling, and M. M. Kasliwal, Astron. Astrophys. **615,** A132 (2018).

[30] B. Abbott *et al.* (LIGO Scientific and Virgo Collaborations), Astrophys. J. Lett. **892,** L3 (2020).

[31] N. Farrow, X.-J. Zhu, and E. Thrane, Astrophys. J. **876,** 18 (2019).

[32] M. L. Rawls, J. A. Orosz, J. E. McClintock, M. A. P. Torres, C. D. Bailyn, and M. M. Buxton, Astrophys. J. **730,** 25 (2011).

[33] F. Ozel, D. Psaltis, R. Narayan, and A. S. Villarreal, Astrophys. J. **757,** 55 (2012).

[34] J. Antoniadis, P. C. Freire, N. Wex, T. M. Tauris, R. S. Lynch *et al.*, Science **340,** 6131 (2013).

[35] Z. Arzoumanian *et al.* (NANOGrav Collaboration), Astrophys. J. Suppl. Ser. **235,** 37 (2018).

[36] P. Demorest, T. Pennucci, S. Ransom, M. Roberts, and J. Hessels, Nature (London) **467,** 1081 (2010).

[37] E. Fonseca *et al.*, Astrophys. J. Lett. **915,** L12 (2021).

[38] B. Margalit and B. D. Metzger, Astrophys. J. Lett. **850,** L19 (2017).

[39] L. Rezzolla, E. R. Most, and L. R. Weih, Astrophys. J. **852,** L25 (2018).

[40] M. Shibata, E. Zhou, K. Kiuchi, and S. Fujibayashi, Phys. Rev. D **100,** 023015 (2019).

[41] J. M. Lattimer, Universe **5,** 159 (2019).

[42] J. G. Martinez, K. Stovall, P. C. C. Freire, J. S. Deneva, F. A. Jenet, M. A. McLaughlin, M. Bagchi, S. D. Bates, and A. Ridolfi, Astrophys. J. **812,** 143 (2015).

[43] P. Lazarus *et al.*, Astrophys. J. **831,** 150 (2016).

[44] M. Dominik, K. Belczynski, C. Fryer, D. Holz, E. Berti, T. Bulik, I. Mandel, and R. O'Shaughnessy, Astrophys. J. **759,** 52 (2012).

[45] L. Blanchet, Living Rev. Relativity **17,** 2 (2014).

[46] K. Hotokezaka, K. Kyutoku, H. Okawa, and M. Shibata, Phys. Rev. D **91,** 064060 (2015).

[47] T. Hinderer *et al.*, Phys. Rev. Lett. **116,** 181101 (2016).

[48] J. Steinhoff, T. Hinderer, A. Buonanno, and A. Taracchini, Phys. Rev. D **94,** 104028 (2016).

[49] S. Akcay, S. Bernuzzi, F. Messina, A. Nagar, N. Ortiz, and P. Rettegno, Phys. Rev. D **99,** 044051 (2019).

[50] A. Nagar, F. Messina, P. Rettegno, D. Bini, T. Damour, A. Geralico, S. Akcay, and S. Bernuzzi, Phys. Rev. D **99,** 044007 (2019).

[51] S. Bernuzzi, A. Nagar, T. Dietrich, and T. Damour, Phys. Rev. Lett. **114,** 161103 (2015).

[52] T. Dietrich and T. Hinderer, Phys. Rev. D **95,** 124006 (2017).

[53] A. Nagar and P. Rettegno, Phys. Rev. D **99,** 021501 (2019).

[54] T. Dietrich, S. Bernuzzi, and W. Tichy, Phys. Rev. D **96,** 121501 (2017).

[55] K. Kawaguchi, K. Kiuchi, K. Kyutoku, Y. Sekiguchi, M. Shibata, and K. Taniguchi, Phys. Rev. D **97,** 044044 (2018).

[56] T. Dietrich *et al.*, Phys. Rev. D **99,** 024029 (2019).

[57] T. Dietrich, A. Samajdar, S. Khan, N. K. Johnson-McDaniel, R. Dudi, and W. Tichy, Phys. Rev. D **100,** 044003 (2019).

[58] T. Dietrich, T. Hinderer, and A. Samajdar, Gen. Relativ. Gravit. **53,** 27 (2021).

[59] S. Bernuzzi, A. Nagar, M. Thierfelder, and B. Brugmann, Phys. Rev. D **86,** 044030 (2012).

[60] K. Hotokezaka, K. Kyutoku, Y.-i. Sekiguchi, and M. Shibata, Phys. Rev. D **93,** 064082 (2016).

[61] T. Narikawa and N. Uchikata, arXiv:2205.06023.

[62] A. Buonanno and T. Damour, Phys. Rev. D **59,** 084006 (1999).

[63] A. Buonanno and T. Damour, Phys. Rev. D **62,** 064015 (2000).

[64] B. D. Lackey, S. Bernuzzi, C. R. Galley, J. Meidam, and C. Van Den Broeck, Phys. Rev. D **95,** 104036 (2017).

[65] B. D. Lackey, M. Pürrer, A. Taracchini, and S. Marsat, Phys. Rev. D **100,** 024002 (2019).

[66] R. Gamba, S. Bernuzzi, and A. Nagar, Phys. Rev. D **104,** 084058 (2021).

[67] D. P. Mihaylov, S. Ossokine, A. Buonanno, and A. Ghosh, Phys. Rev. D **104,** 124087 (2021).

[68] J. Lange, R. O'Shaughnessy, and M. Rizzo, arXiv:1805.10457.

[69] M. Favata, Phys. Rev. Lett. **112,** 101101 (2014).

[70] L. Wade, J. D. E. Creighton, E. Ochsner, B. D. Lackey, B. F. Farr, T. B. Littenberg, and V. Raymond, Phys. Rev. D **89,** 103012 (2014).

[71] R. Dudi, F. Pannarale, T. Dietrich, M. Hannam, S. Bernuzzi, F. Ohme, and B. Brügmann, Phys. Rev. D **98,** 084061 (2018).

[72] A. Samajdar and T. Dietrich, Phys. Rev. D **98,** 124030 (2018).

[73] A. Samajdar and T. Dietrich, Phys. Rev. D **100,** 024046 (2019).

[74] R. Gamba, M. Breschi, S. Bernuzzi, M. Agathos, and A. Nagar, Phys. Rev. D **103,** 124015 (2021).

[75] G. Ashton and T. Dietrich, arXiv:2111.09214.

[76] L. Lehner, S. L. Liebling, C. Palenzuela, O. L. Caballero, E. O'Connor, M. Anderson, and D. Neilsen, Classical Quantum Gravity **33,** 184002 (2016).

[77] T. Dietrich, M. Ujevic, W. Tichy, S. Bernuzzi, and B. Bruegmann, Phys. Rev. D **95,** 024029 (2017).

[78] D. Radice, A. Perego, K. Hotokezaka, S. A. Fromm, S. Bernuzzi, and L. F. Roberts, Astrophys. J. **869,** 130 (2018).

[79] S. Bernuzzi et al., Mon. Not. R. Astron. Soc. **497,** 1488 (2020).

[80] L. J. Papenfort, E. R. Most, S. Tootle, and L. Rezzolla, Mon. Not. R. Astron. Soc. **513,** 3646 (2022).

[81] W. Tichy, Classical Quantum Gravity **26,** 175018 (2009).

[82] W. Tichy, Phys. Rev. D **86,** 064024 (2012).

[83] T. Dietrich, N. Moldenhauer, N. K. Johnson-McDaniel, S. Bernuzzi, C. M. Markakis, B. Brügmann, and W. Tichy, Phys. Rev. D **92,** 124007 (2015).

[84] W. Tichy, A. Rashti, T. Dietrich, R. Dudi, and B. Brügmann, Phys. Rev. D **100,** 124046 (2019).

[85] J. W. York, Jr., Phys. Rev. Lett. **82,** 1350 (1999).

[86] W. Tichy, Phys. Rev. D **84,** 024041 (2011).

[87] B. Brügmann, J. A. Gonzalez, M. Hannam, S. Husa, U. Sperhake, and W. Tichy, Phys. Rev. D **77,** 024027 (2008).

[88] M. Thierfelder, S. Bernuzzi, and B. Brügmann, Phys. Rev. D **84,** 044012 (2011).

[89] T. Dietrich, S. Bernuzzi, M. Ujevic, and B. Brügmann, Phys. Rev. D **91,** 124041 (2015).

[90] S. Bernuzzi and T. Dietrich, Phys. Rev. D **94,** 064062 (2016).

[91] T. Dietrich, D. Radice, S. Bernuzzi, F. Zappa, A. Perego, B. Brügmann, S. V. Chaurasia, R. Dudi, W. Tichy, and M. Ujevic, Classical Quantum Gravity **35,** 24LT01 (2018).

[92] S. Bernuzzi and D. Hilditch, Phys. Rev. D **81,** 084003 (2010).

[93] D. Hilditch, S. Bernuzzi, M. Thierfelder, Z. Cao, W. Tichy, and B. Brügmann, Phys. Rev. D **88,** 084057 (2013).

[94] C. Bona, J. Massó, J. Stela, and E. Seidel, in The Seventh Marcel Grossmann Meeting: On Recent Developments in Theoretical and Experimental General Relativity, Gravitation, and Relativistic Field Theories, edited by R. T. Jantzen, G. M. Keiser, and R. Ruffini (World Scientific, Singapore, 1996).

[95] M. Alcubierre, B. Bruegmann, P. Diener, M. Koppitz, D. Pollney, E. Seidel, and R. Takahashi, Phys. Rev. D **67,** 084023 (2003).

[96] J. R. van Meter, J. G. Baker, M. Koppitz, and D.-I. Choi, Phys. Rev. D **73,** 124011 (2006).

[97] J. S. Read, B. D. Lackey, B. J. Owen, and J. L. Friedman, Phys. Rev. D **79,** 124032 (2009).

[98] A. Bauswein, H. T. Janka, and R. Oechslin, Phys. Rev. D **82,** 084043 (2010).

[99] N. Moldenhauer, C. M. Markakis, N. K. Johnson-McDaniel, W. Tichy, and B. Brügmann, Phys. Rev. D **90,** 084043 (2014).

[100] E. Newman and R. Penrose, J. Math. Phys. (N.Y.) **3,** 566 (1962).

[101] C. Reisswig and D. Pollney, Classical Quantum Gravity **28,** 195015 (2011).

[102] T. Dietrich, S. Bernuzzi, B. Bruegmann, and W. Tichy, in Proceedings of the 26th Euromicro International Conference on Parallel, Distributed and Network-based Processing (PDP 2018), 2018 (Cambridge University Press, Cambridge, England, 2018), pp. 682–689, arXiv:1803.07965.

[103] L. London, S. Khan, E. Fauchon-Jones, C. García, M. Hannam, S. Husa, X. Jiménez-Forteza, C. Kalaghatgi, F. Ohme, and F. Pannarale, Phys. Rev. Lett. **120,** 161102 (2018).

[104] S. Khan, F. Ohme, K. Chatziioannou, and M. Hannam, Phys. Rev. D **101,** 024056 (2020).

[105] R. Cotesta, S. Marsat, and M. Pürrer, Phys. Rev. D **101,** 124040 (2020).

[106] LIGO Scientific Collaboration, LIGO Algorithm Library—LALSuite, free software (GPL) (2018).

[107] A. Matas et al., Phys. Rev. D **102,** 043023 (2020).

[108] J. E. Thompson, E. Fauchon-Jones, S. Khan, E. Nitoglia, F. Pannarale, T. Dietrich, and M. Hannam, Phys. Rev. D **101,** 124059 (2020).

[109] M. Hannam, P. Schmidt, A. Bohé, L. Haegel, S. Husa, F. Ohme, G. Pratten, and M. Pürrer, Phys. Rev. Lett. **113,** 151101 (2014).

[110] S. Khan, S. Husa, M. Hannam, F. Ohme, M. Pürrer, X. Jiménez Forteza, and A. Bohé, Phys. Rev. D **93,** 044007 (2016).

[111] A. Bohé et al., Phys. Rev. D **95,** 044028 (2017).

[112] J. Steinhoff, T. Hinderer, T. Dietrich, and F. Foucart, Phys. Rev. Research **3,** 033129 (2021).